Conference on Modelling Fluid Flow (CMFF'22)
The 18th International Conference on Fluid Flow Technologies
Budapest, Hungary, August 30-September 2, 2022

EFFECTS OF LARGE PARTICLES IN PIPE FLOW AT LOW AND MODERATE REYNOLDS NUMBERS

Johan REVSTEDT[1], Dragana ARLOV[2], Fredrik INNINGS[3]

[1] Corresponding Author. Department of Energy Sciences, Faculty of Engineering, Lund University, P.O. Box 118, SE-22100 Lund, Sweden
Phone.: +46 46 222 4302, E-mail: johan.revstedt@energy.lth.se
[2] Tetra Pak Processing Systems AB. E-mail: dragana.arlov@tetrapak.com
[3] Tetra Pak Processing Systems AB. E-mail: fredrik.innings@tetrapak.com

ABSTRACT

The presence of solid particles in a Newtonian liquid flow will affect the properties of the flow. For small particles these effects are fairly well understood. However, the behaviour of liquids laden with large particles are less well understood and even more so if the carrier liquid is a non-Newtonian fluid. In the present study we consider large particles of spherical shape. By large is here meant particles that are of the same size as the large scale length scales of the flow and larger. We are considering how particles volume fraction affects parameters such as pressure drop and velocity distribution in the pipe flow. The simulations are performed using a finite difference based in-house software and the particles are represented using an virtual boundary method. The size of the spherical particles is about 1/6 of the pipe diameter and the volume fraction is varied between 5 and 20%. The fluid is either Newtonian or shear thinning modelled using a power law expression.

Keywords: non-Newtonian, particles, pipe flow, virtual boundary method

NOMENCLATURE

$\underline{U}$	$[-]$	particle linear velocity
C	$[-]$	a constant
D	$[m]$	pipe diameter
Fr	$[-]$	Froude number
K	$[kg/(ms^{2-n}]$	consistency index
R	$[-]$	pipe radius
Re	$[-]$	Reynolds number
t	$[-]$	time
U_B	$[m/s]$	bulk velocity
V	$[-]$	volume
ψ	$[-]$	distance function
$\underline{u}$	$[-]$	velocity vector
d	$[m]$	particle diameter
f	$[-]$	Darcy friction factor
k	$[-]$	spring coefficient
n	$[-]$	power-law index
p	$[-]$	pressure
r	$[-]$	radial coordinate
x	$[-]$	coordinate
$\underline{v}$	$[-]$	boundary target velocity
$\underline{\underline{S}}$	$[-]$	strain rate tensor
α	$[-]$	shape coefficient
β	$[-]$	shape coefficient
$\dot{\gamma}$	$[-]$	absolute value of strain rate
ε	$[-]$	Levi-Civita symbol
η	$[-]$	damping coefficient
μ	$[-]$	viscosity factor
Φ	$[-]$	source term
ϕ	$[-]$	particle volume fraction
ρ	$[kg/m^3]$	density
τ_w	$[Pa]$	wall shear stress
$\underline{\delta}$	$[-]$	particle overlap
$\underline{\omega}$	$[-]$	particle angular velocity
$\underline{\xi}$	$[-]$	distance vector
$\underline{\mathcal{F}}$	$[-]$	particle force
$\underline{\mathcal{T}}$	$[-]$	particle torque

Subscripts and Superscripts

MR	Metzner-Reed
B	bulk
s	single phase
rel	relative
c	contact
f	fluid
h	hydrodynamic
i, j, k	Cartesian tensor indices
p	particle

INTRODUCTION

Introducing solid particles to a Newtonian liquid flow will alter the properties of the flow compared to a pure the liquid. For small particles these effects are fairly well understood and models, for example for the pressure drop in particle laden pipe flows have been present for a long time. In terms of modelling the effects are often represented in terms of a modified viscosity. This approach to modelling dates back

to the work of Einstein [1, 2] who formulated the viscosity of particle suspension as a function of the volume fraction of particles. Einstein's formulation is, however, only valid for dilute suspensions containing small particles. An extension of this, which is valid for larger volume fractions was proposed by Eilers [3]. Again, Eilers' correlation fits well for small particles which have been confirmed by several studies. Essentially, considering laminar flow, the Darcy friction factor for this type of flow would vary with Reynolds number in a similar way as a flow without particles. Hence, formulating a Reynolds number based on the viscosity from the Eilers formula the curves would collapse on top of each other and the normal Moody chart could be used to predict the pressure drop. This works well for small particles and is also surprisingly accurate for fairly large particles provided the volume fraction is low.

However, liquid flows laden with large particles are less well understood and even less so if the carrier liquid is non-Newtonian. By large is here meant particles that are of the same size as the large scale length scales of the flow and larger. For pipe flows (which is the focus of this study) this would mean particle with hydraulic diameters of about 15 to 20% of the pipe diameter and larger. In such flows several factors influence the flow behaviour. For example, one can find that the pressure drop is not just dependent on particle volume fraction but also on particle shape and size distribution. There are also indications that the presence of particles has a strong influence on the heat transfer in a pipe, either amplifying or attenuating it depending on several parameters.

Although, the influence of larger particles has been less well studied some investigations, both experimental and numerical, can be found in the literature. In a fairly extensive experimental study Matas et al [4] considered particle laden pipe flows with particle volume fractions up to about 35%. They also considered a wide range of particle sizes, particle diameter to pipe diameter (d/D) in the range 0.1 to about 0.003. The focus of their study was how the transition to turbulence is affected by particle content. Two distinct behaviours were observed depending on particle size. For smaller particles the transition was delayed, while for larger particles the transition occurred at a lower Reynolds number that for a single phase flow. Turbulence transition was also studied by Agrawal et al [5]. They considered a particle size ratio d/D of 0.05 and volume fractions up to 24%. Measuring the pressure drop and then considering the Darcy friction factor, they found that even at low volume fractions (about 2%) the friction factor switched from the laminar behaviour, to a turbulent behaviour with friction faction values somewhat higher than for single phase flow, at a lower Reynolds number than for a liquid without particles. Lashgari et al [6] considered numerically a channel flow with particle volume fractions up to 30% with a channel height to particle diameter (H/d) of 10. They found that depending on Reynolds number and volume fraction the flow could be divided into three regimes: laminar like (small Re and volume fraction (ϕ)), turbulent like (large Re and small ϕ) and inertial shear thickening (large ϕ). The turbulent structures of particle laden pipe flows were studied numerically by Wu et al [7]. Also in this studied, a relative particle size of 10 was used and the Reynolds number was fixed to 4900. The results show that the presence of particles attenuated the maximum streamwise fluctuations close to the wall while fluctuations in the radial and tangential directions were increase in the same region and that these effects increased at higher volume fractions. The reason for the increase in radial and tangential fluctuations, according to Wu et al [7], is the small vortices induced by the particles in the region close to the wall. Also, the position of maximum radial fluctuation was shifted slightly towards the wall.

Our focus will be on laminar and moderately turbulent flows considering both Newtonian and non-Newtonian carrier fluids. The overall aim of this study is to further increase the understanding of particle laden flows, in particular pipe flows with large particles.

MATHEMATICAL DESCRIPTION

The momentum equation governing the incompressible flow of a non-Newtonian (shear thinning or shear thickening) fluid can on non-dimensional be written as

$$\frac{\partial u_i}{\partial t} + u_j \frac{\partial u_i}{\partial x_j} = -\frac{\partial p}{\partial x_i} + \mu \left(\frac{\partial^2 u_i}{\partial x_j^2} \right) + \left[\frac{\partial \mu}{\partial x_j} \left(\frac{\partial u_i}{\partial x_j} + \frac{\partial u_j}{\partial x_i} \right) \right] + \Phi_i. \quad (1)$$

The rheology of the fluid is modelled using a power-law expression and the viscosity coefficient in eq. (1) can then be described as

$$\mu = \frac{1}{Re} \dot{\gamma}^{n-1} \quad (2)$$

where n is the power law index and with shear rate, γ, formulated using an isotropic expression, i.e.

$$\dot{\gamma} = \sqrt{S_{ij} S_{ij}} \quad (3)$$

The Reynolds number for a power law fluid in a pipe flow, based on the bulk velocity, U_B, pipe diameter, D and the consistency index of the fluid may be written as

$$Re = \frac{\rho_f U_B^{2-n} D^n}{K} \quad (4)$$

Turbulence modelling

In the present study both laminar and turbulent flows are considered. Turbulence is handled using an implicit large eddy simulation (LES) method. The sub-grid scale stresses are handled using the dissip-

ative nature of the truncation error in the discretisation of the convective terms. Here we use the third order upwind scheme of Kawamura and Kuwahara [8]. This approach has been successfully used in several previous studies, e.g. [9] and, as is shown below works well also in this case.

Virtual boundary method

The source terms Φ_i are introduced to represent solid boundaries, i.e. they replace the boundary conditions on the solid body surface. In this case the sources Φ_i are computed so as to satisfy the local boundary conditions. Hence, the source terms will only be non-zero at the location of the boundary. However, discretising the computational domain will in general lead to that the presence of the boundary must be represented by source terms in positions away from the actual boundary location. This can be achieved in different ways, for example by approximating the Dirac function by a normalised Gaussian distribution [10] or by assuming a certain distribution of the velocity field normal to the boundary [11]. In this work we employ the method developed by Revstedt [9] in which the source term is accumulated over the time steps and iterations within each time step. Hence, the following expression for the contribution to the discretised source terms in the mth iteration is written as:

$$\Delta\overline{\Phi}_i^m = C_1 \frac{v_i - u_i}{\Delta t} e^{-C_2\psi^2} \tag{5}$$

where C_1 and C_2 are positive constants, v_i is the target velocity of the solid surface and ψ is a positive function which should increase rapidly with increasing distance from the solid boundary. Hence, inside the body ψ will be set to zero and far away from the body it will have a large positive value, typically 10^6. Several strategies for setting the ψ-function may be used but here a step function is employed. Finally the magnitude of the source terms in the mth iteration is given by

$$\overline{\Phi}_i^m = \overline{\Phi}_i^{m-1} + \Delta\overline{\Phi}_i^m \tag{6}$$

Numerical method

The incompressible Navier-Stokes equations are discretised on a system of locally refined staggered Cartesian grids (e.g. Fuchs and Zhao [12]). The terms of the momentum and continuity equations are approximated by finite-differences. Basically, one may use finite-differences of any order. Here, we use upwind finite-differences of first- or third-order accuracy. The lower order scheme (first order for the convective terms and second order for the others) implies that the low order terms dominate, leading to a high level of numerical dissipation. Using directly higher order (third and fourth order approximations, respectively), leads to a less robust solver with considerably slower convergence rate. To combine numerical efficiency with higher order accuracy, we introduce the higher order terms as a "single-step" defect correction [13].

The time integration is done by a three level implicit scheme. In each time step, the system of equations is solved iteratively using a Multi-grid solver. Local grid refinements are a part of the multi-grid structure and the boundary conditions are interpolated from the next coarser level using fourth order linear interpolation.The relaxation scheme within the Multi-grid solver comprises of point wise relaxation of the momentum equations coupled with a point wise smoothing of the continuity equation. At the latter step, both the velocity vector and the pressure are corrected so that the residuals of the momentum equations shall not be changed as the continuity equation is satisfied. This approach is equivalent to an approximate diagonalisation of the system of equations [12].

Particle motion and interaction

The linear and angular velocities of each individual particle are governed by the following equations:

$$\frac{dU_i}{dt} = \left(1 - \frac{\rho_f}{\rho_p}\right)\frac{1}{Fr_i^2} - \alpha\frac{\rho_f}{\rho_p}\left(\mathcal{F}_i^{(h)} - \mathcal{F}_i^{(c)}\right) \tag{7}$$

$$\frac{d\omega_i}{dt} = \beta\frac{\rho_f}{\rho_p}\left(\mathcal{T}_i^{(h)} - \mathcal{T}_i^{(c)}\right) \tag{8}$$

where (h) and (c) denotes the hydrodynamic and contact forces, respectively, and α and β are coefficients dependent on the particle shape. For a sphere $\alpha = 6/\pi$ and $\beta = 10\alpha$. The hydrodynamic force is determined by integrating the discretised source term $\overline{\Phi}_i$ from eq. (5) in a volume around the particle.

$$\mathcal{F}_i^{(h)} = \int \overline{\Phi}_i dV. \tag{9}$$

The hydrodynamic torque is calculated in a similar way

$$\mathcal{T}_i^{(h)} = \int \varepsilon_{ijk}\overline{\Phi}_k \xi_j dV. \tag{10}$$

To find the contact forces we use a soft sphere approach similar to the one developed by Costa et al [14]. One can then on non-dimensional form write the force for each particle contact as

$$\mathcal{F}_i^{(c)} = -k\delta_i - \eta u_{i,\mathrm{rel}} \tag{11}$$

Hence, each contact is modelled as a spring and a damper mounted in parallel, with the spring and damping coefficients being evaluated based on the effective particle mass, restitution coefficient and the allowed contact time. The torque generated by a collision is calculated as

$$\mathcal{T}_i^{(c)} = \varepsilon_{ijk}\mathcal{F}_k^{(c)}\xi_j \tag{12}$$

COMPUTATIONAL SET-UP

The computational domain consists of a circular pipe created in a rectangular domain using an virtual boundary method. The length of the pipe is about 6 pipe diameters (D). However, due to how the domain decomposition is done the length to diameter ratio of the pipe may vary somewhat. At the inflow and outflow of the pipe cyclic boundary conditions are used both for the continuous phase and the particles. In the simulations we consider spherical particles of size $d/D = 0.171$. The density ratio is set to unity, i.e. the particles are neutrally buoyant. The computational mesh is Cartesian and structured. Two levels of resolution have been used depending on particle size and flow situation. For the laminar flow the resolution is set to $\Delta x = 0.0625$ which corresponds to about 94 cells over the pipe diameter. For turbulent flow the resolution is $\Delta x = 0.03125$ which corresponds to about 188 cells over the pipe diameter. The temporal resolution in the laminar cases is $\Delta t = 0.01$ and in the turbulent cases $\Delta t = 0.005$. Initially the liquid velocity is set equal to the bulk velocity in the whole pipe. Particles are initially ordered in rows and their velocity is set equal to the liquid velocity. All simulations have been run for 40000 time steps before sampling of data is initiated in order to let the solution develop sufficiently. Sampling was done over an additional 100000 time steps.

Four fluids with different degrees of shear thinning are considered, the power-law index ranging from 0.4 to 1.0. For all fluids flows with Reynolds numbers in the range 250 to 2000 are studied and for $n = 0.4$ and $n = 1.0$ also turbulent flows are considered, i.e. $4000 \leq Re \leq 16000$.

Throughout the study a modified Reynolds number is used

$$Re_{\mathrm{MR}} = \frac{\rho_f U_B^{2-n} D^n}{K\left(\frac{3n+1}{4n}\right)^n 8^{1-n}} \tag{13}$$

This Reynolds number was first presented by Metzner and Reed [15] in order to fit friction factor data for non-Newtonian fluids to the Moody chart.

Code validation

Figure 1 the average velocity and Reynolds normal stresses in a pipe flow at Re=11700 compared to direct numerical simulation (DNS) data from El Khoury et al [16]. As can be seen, our results agree very well with the DNS data indicating that our resolution is sufficient for the turbulent cases considered, event hough the viscous sublayer is not fully resolved in our simulations. Also, our simulation underpredicts the friction losses, in terms of Darcy friction factor, by about 10%.

To further show the capability of the code to predict the resistance in a pipe flow the Darcy friction factor as a function of the Metzner-Reed Reynolds number is depicted in Figure 2 for the range $250 \leq Re_{\mathrm{MR}} \leq 16000$ for the Newtonian fluid. However, the friction factor for a shear-thinning fluid ($n = 0.4$)

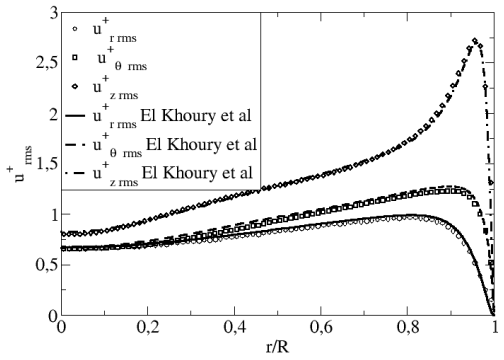

Figure 1. RMS of velocity fluctuations in a pipe flow with Re=11700 compared to DNS data by El Khoury et al [16]

at $Re_{\mathrm{MR}} = 4000$ is also shown. The solid line in Fig. 2 is the classical $f = 64/Re$ line in the laminar regime. The dashed line is the Haaland equation for a smooth pipe and the dot-dashed line is the extension of the turbulent friction factor by Wilson and Thomas [17] to a power-law fluid with $n = 0.4$. As can be seen, the friction factor is slightly underpredicted in the whole range which is most probably caused by the virtual boundary method introducing a small error in the description of the pipe wall, i.e. the pipe appears slightly larger it should be.

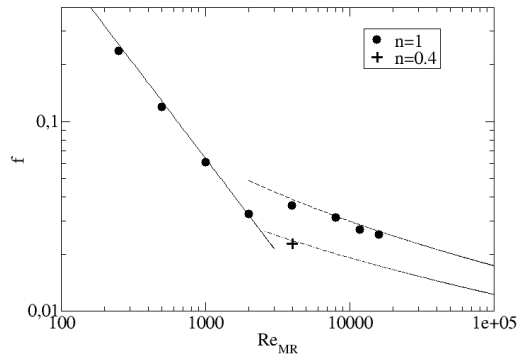

Figure 2. Darcy friction factor without particles

The two grid resolutions used in this study corresponds to 16 or 32 cells over the particle diameter. A previous study on free falling cubical particles [18] shows that 16 cells is sufficient to describe the particle with reasonable accuracy.

RESULTS

Introducing particles to a pipe flow one expects flow resistance to increase, which is indeed the case. Figure 3 depicts the Darcy friction factor ($f = \frac{8\tau_w}{\rho_f U_B^2}$) as a function of the Reynolds number for a New-

tonian fluid. Already at a particle volume fraction $\phi_B = 0.05$ the friction factor is noticeably higher than without particles in a laminar flow. Increasing the volume fraction of particles will further increase the resistance. One may note that in the laminar regime the decrease in friction factor with increasing Reynolds number is still linear in the Moody chart, although with a slope that is dependant on volume fraction. For the turbulent regime the behaviour is somewhat different. For the lowest volume fraction the particles seem to only have a minor influence on the resistance and the friction factor is decreasing with increasing Reynolds number, as it would for a flow without particles. However, increasing the volume fraction to 10 and 20% a different behaviour emerges. Not only is the resistance much higher for a given Reynolds number but the friction factor is now constant or even slightly increasing with Reynolds number. We believe the explanation for this to be that at $\phi_B = 0.05$ the interaction between particles is negligible while for higher volume fractions the particles are more often in contact which strongly increases the resistance. Comparing to the the experimental results of Agrawal et al [5] we find that the friction factors in their collapses nicely on the Hagen-Poiseuille solution in the laminar regime with the proper scaling of the Reynolds number while our results deviates significantly from that. The reason for that is that they use much smaller particles for which effective viscosity models, such as Eilers' model [3], are appropriate, which is not the case for larger particles.

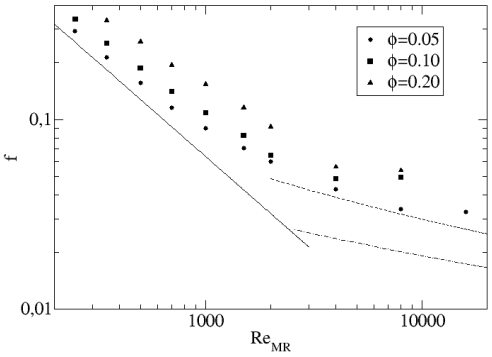

Figure 3. Darcy friction factor as a function of Reynolds number for spherical particles in a fluid with n=1

Comparing the Newtonian results with the resistance of the shear thinning fluid, depicted in Figure 4, the behaviour in the laminar regime is the same in the sense that increasing the volume fraction increases the resistance. Also the behaviour with increasing Reynolds is similar. In the turbulent regime the friction factor falls below the minimum limit for a Newtonian fluid, which would be expected since friction factor is a function of the degree of shear thinning in this range even when using the Metzner & Reed Reynolds number. However, in this case the almost constant friction factor for Re=8000 and beyond appears already at $\phi_B = 0.05$.

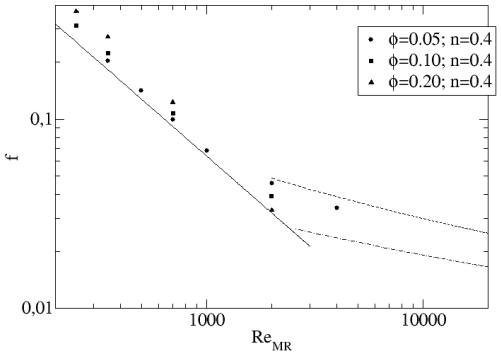

Figure 4. Darcy friction factor as a function of Reynolds number for spherical particles in a fluid with n=0.4

As could be seen from Figs. 3 and 4 there is a difference in friction factor between the Newtonian case and $n = 0.4$. Taking a closer look at how the friction factor varies with degree of shear thinning and Reynolds number, which is shown in Figure 5, one can see that for a low Reynolds number (350) the effect on the friction factor is quite moderate, especially for $\phi = 0.05$ where the value at $n = 0.4$ is about 95% of the Newtonian value. However, the effect of shear thinning seems to get more pronounced with increasing volume fraction and at $\phi = 0.20$ the value at $n = 0.4$ is about 80% of the Newtonian one. The influence of Reynolds number is also very strong leading to a substantial difference in resistance at Re=2000. Comparing the velocity profiles for $n = 0.4$, depicted in Figure 6, one finds for the lowest volume fraction that the maximum velocity decreases as the Reynolds number increases. This also means that the velocity profile in the centre part of the pipe ($r/R \leq 0.5$) gets flatter while the portion of the pipe with a higher velocity gradient gets larger. A interesting observation is that up to $Re = 1000$ the velocity gradient close to the wall is unchanged, meaning that the resistance should be dependant on a constant to the power n divided by Reynolds number in this regime. Increasing the Reynolds number to 2000 results in a change in the velocity distribution such that the shear rate close to the wall increases and one would therefore expect that for this case the friction factor would not fall on the same line in the Moody chart as the lower Reynolds numbers, which is indeed the case considering Fig. 4. It also indicates that the at $Re = 2000$ is, if not fully turbulent, at least in a transition state. Considering instead the case $\phi = 0.20$ the trend is the same concern-

ing the centre line velocity. However, the shapes of the velocity distributions are distinctly different compared to $\phi = 0.05$. For Reynolds number up to 700 one observes to separate behaviours in the inner and outer half of the pipe. In the inner part ($r/R < 0.5$) the velocity profile is fairly flat, much like for lower particle volume fraction, but there is also a plateau in the outer part of the pipe, which is most pronounced at $Re = 700$. Again one observes that $Re = 2000$ differs from the other cases with an almost constant velocity for $r/R < 0.8$. Once more, even though there is a significant Reynolds number effect on the velocity distribution, close to the wall the velocity gradient shows only a minor Reynolds number dependence. This is consistent with what is found in Fig. 4. Further insight in the differences in velocity distribution may be gained by considering the distribution of particle volume fraction along the radius. This is depicted in Figure 7 for $n = 0.4$ at $\phi = 0.05$ and $\phi = 0.2$. For $\phi = 0.05$ at $Re = 1000$ and below the particles are mainly located in the outer part of the pipe with the peak of volume fraction gradually moving towards lower radius with increasing Reynolds number as can be seen in the upper graph of Fig. 7. Again the $Re = 2000$ deviates significantly from this pattern and instead the particles are almost evenly distributed over the pipe radius. Turning the attention to the cases with $\phi = 0.20$ a totally different pattern emerges. Here particles tend to cluster close to the centre line with a secondary peak at about the same position as for the lower volume fraction. However, this situation is drastically altered at $Re = 700$ where most of the particles a located closer to the pipe wall. It is also interesting to note that there is no drastic change at $Re = 2000$ instead the distribution of particle volume is qualitatively similar to the one at $Re = 700$ put shifted to a lower radius.

Turbulent regime

For the turbulent regime $Re > 2000$ it is evident from Fig. 3 that the flow behaves differently. For the Newtonian case a decrease in friction factor is seen going from $Re = 2000$ to $Re = 4000$ for all volume fractions and for $\phi = 0.05$ this decrease continues up to $Re = 8000$. The particle here have only a minor influence on the resistance. However, increasing the volume fraction a significant influence on the resistance from the presence of particles is seen and also that the friction factor stops decreasing already beyond $Re = 4000$. For the shear thinning fluid ($n = 0.4$) a large increase in resistance compared to a flow without particles is seen already at $Re = 4000$. The relative increase in friction factor compared to the case without particles is summarised in Table 1.

From Table 1 it is evident that even a moderate amount of particles will have a substantial influence on the resistance also in a pipe flow. However, the increase is still less than in the laminar regime, where for $\phi = 0.05$ the increase due to particles is about 50% at $Re = 700$ and 100% for $\phi = 0.20$ at

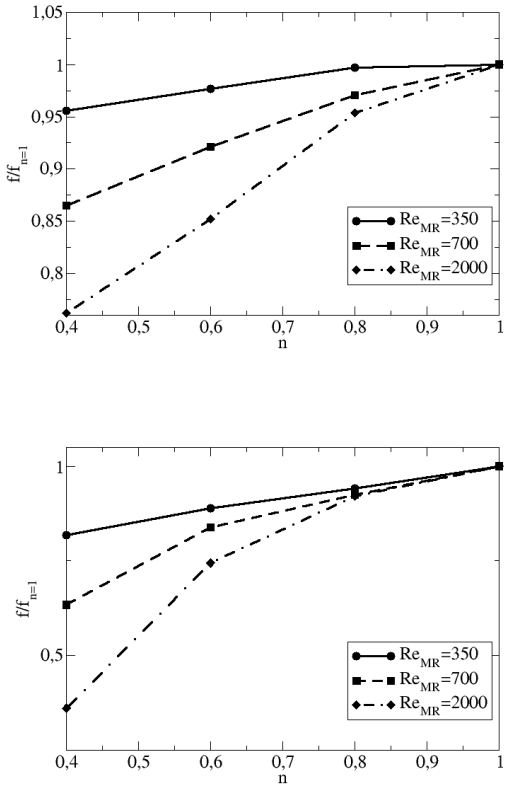

Figure 5. Friction factor normalised with the value for $n = 1$ as a function of as a function of degree of shear thinning for some Reynolds numbers in the laminar regime for $\phi = 0.05$ (upper) and $\phi = 0.20$ (lower)

the same Reynolds number. Furthermore, the influence increases for a shear thinning fluid. Some insight on this matter can be achieved by considering the radial distribution of the particle phase. Figure 8 depicts the local particle volume fraction normalised with the bulk value along the radius for Reynolds numbers 4000 and 8000 for the Newtonian fluid. At $Re = 4000$ the particles tend to be located more towards the centre of the pipe but with a tendency for increased volume fraction close to the wall as the overall volume fraction is increased. This will of course influence the flow close to the wall and in turn also the resistance. At $Re = 8000$ the effect is less pronounced and the distribution of the pipe more even especially for $\phi = 0.02$ and still there is a tendency for the particles to locate themselves closer to the wall with increasing ϕ

SUMMARY

Simulations of pipe flow containing relatively large particles have been performed for both laminar and turbulent flow. It can be concluded that the presence of particles will increase the flow resistance for both shear thinning and Newtonian fluids. The level

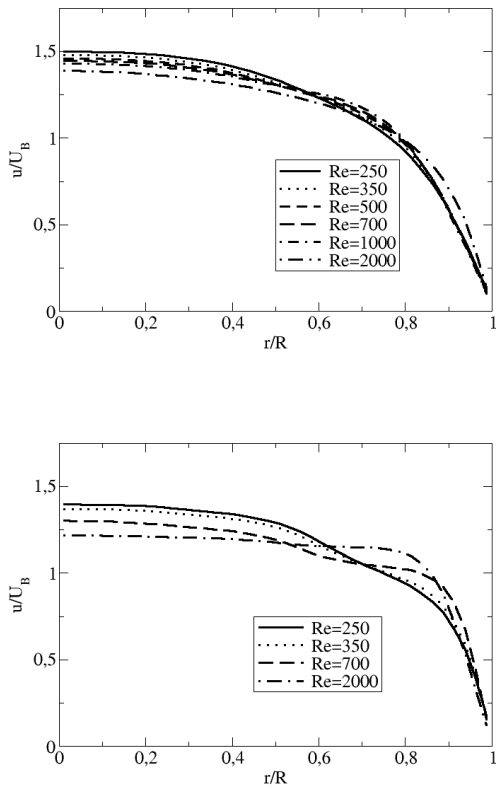

Figure 6. Velocity distribution along the pipe radius at $n = 0.4$ for some Reynolds numbers in the laminar regime for $\phi = 0.05$ (upper) and $\phi = 0.20$ (lower)

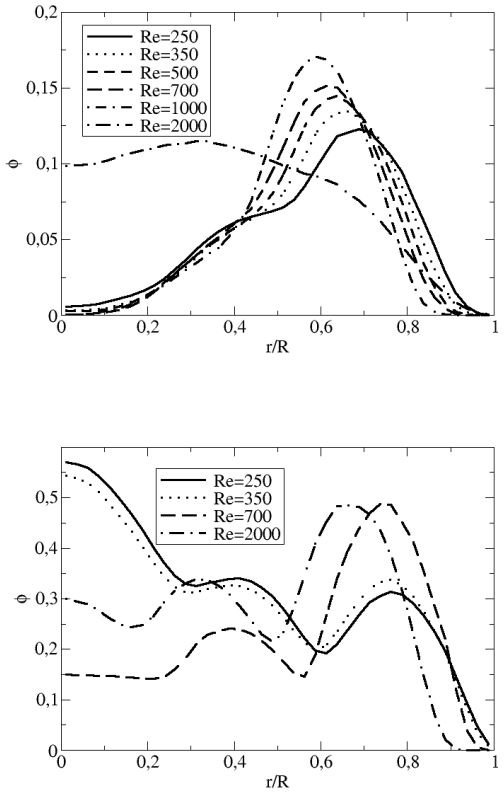

Figure 7. Distribution of particle volume fraction along the pipe radius at $n = 0.4$ for some Reynolds numbers in the laminar regime for $\phi = 0.05$ (upper) and $\phi = 0.20$ (lower)

of increase in resistance depends on the volume fraction as well as the Reynolds number and the degree of shear thinning. In general the effect of volume fraction is larger for a laminar flow with increases in friction factor of up to 100% for 20% particle volume fraction in a Newtonian fluid. A shear thinning fluid will give a smaller resistance than a Newtonian fluid at a given Reynolds number and in the laminar regime this difference increases with increasing Reynolds number. In the turbulent regime there seems to be a threshold effect in as much as a low volume fraction (5%) has no significant effect on the resistance while increasing to 10% increases the resistance significantly. However, at a sufficiently high Reynolds number a low volume fraction will also have a significant effect. Furthermore, it seems that the Reynolds number where this change occurs is lower for a shear thinning fluid. In conclusion, adding large particles to a pipe flow will increase the level of complexity in how that flow behaves. Also, there is a very distinct difference in how the particles alter the flow in the laminar and turbulent regimes, respectively.

ACKNOWLEDGEMENTS

Financial support for this work provided by the Swedish Energy Agency project no. 44266-1 and by Tetra Pak Processing Systems AB. Computational resources were provided by the Swedish National Infrastructure for Computing (SNIC) at NSC and by Lunarc.

REFERENCES

[1] Einstein, A., 1906, "Eine neue Bestimmung der Moleküldimensionen", *Ann Phys*, Vol. 324, pp. 289–306.

[2] Einstein, A., 1911, "Berichtigung zu meiner Arbeit: Eine neue Bestimmung der Moleküldimensionen", *Ann Phys*, Vol. 339, pp. 591–592.

[3] Eilers, H., 1941, "Die Viscosität von Emulsionen hochviskoser Stoffe als Funktion der Konzentration", *Kolloid-Zeitschrift*, Vol. 97, pp. 313–321.

[4] Matas, J.-P., Morris, J., and Guazzelli, E., 2003, "Transition to turbulence in particulate pipe flow", *Phys Rev Lett*, Vol. 90, p. 014501.

Table 1. Darcy friction factor relative to flow without particles

n	ϕ	Re	f/f_s
1	0.05	4000	1.08
1	0.05	8000	1.05
1	0.05	16000	1.29
1	0.10	4000	1.35
1	0.10	8000	1.59
1	0.20	4000	1.56
1	0.20	8000	1.73
0.4	0.05	4000	1.49

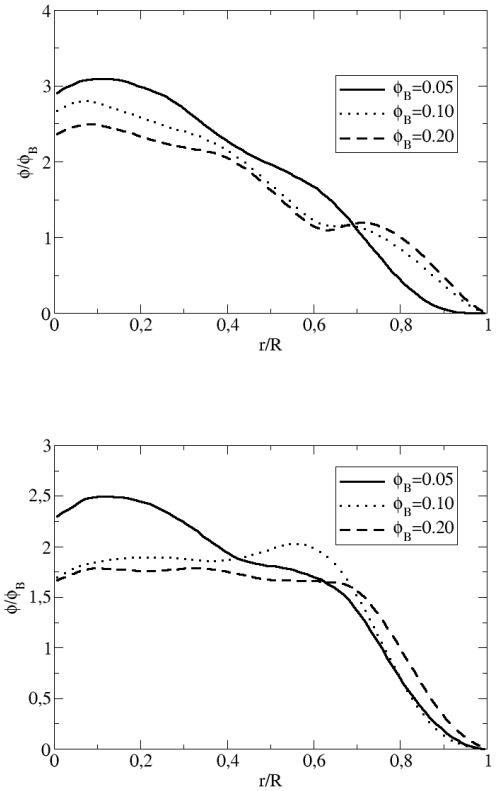

Figure 8. Radial distribution of particle volume fraction for Re = 4000 (upper) and Re = 8000 (lower) for the Newtonian fluid

[5] Agrawal, N., Choueiri, G., and Hof, B., 2019, "Transition to turbulence in particle laden flows", *Phys Rev Lett*, Vol. 122, p. 114502.

[6] Lashgari, I., Picano, F., Breugem, W.-P., and Brandt, L., 2014, "Laminar, turbulent, and inertial shear-tickening regimes in channel flow of neutrally buoyant particle suspensions", *Phys Rev Lett*, Vol. 113, p. 254502.

[7] Wu, T., Shao, X., and Yu, Z., 2011, "Fully resolved numerical simulation of turbulent pipe flows laden with large neutrally-buoyant particles", *J Hydrodynamics*, Vol. 23, pp. 21–25.

[8] Kawamura, T., and Kuwahara, K., 1984, "Computation of high Reynolds number flow around a circular cylinder with surface roughness", *AIAA paper*, Vol. 84-0340.

[9] Revstedt, J., 2013, "Interaction between an incompressible flow and elastic cantilevers of circular cross-section", *Int J Heat Fluid Flow*, Vol. 43, pp. 244–250.

[10] Revstedt, J., 2004, "A virtual boundary method with improved computational efficiency using a multi-grid method", *int J Num Meth Fluids*, Vol. 45 (7), pp. 775–795.

[11] Fadlun, E., Verzicco, R., Orlandi, P., and Modh-Yusof, J., 2000, "Combined Immersed-boundary finite-difference methods for three-dimensinal complex flow situations", *J Comput Phys*, Vol. 161, pp. 35–60.

[12] Fuchs, L., and Zhao, H.-S., 1984, "Solution of three-dimensional viscous incompressible flows by a multi-grid method", *int J Num Meth Fluids*, Vol. 4, pp. 539–555.

[13] Gullbrand, J., Bai, X.-S., and Fuchs, L., 2001, "High-order Cartesian grid method for calculation of incompressible turbulent flow", *int J Num Meth Fluids*, Vol. 36, pp. 539–555.

[14] Costa, P., Boersma, B., Westerweel, J., and Breugem, W.-P., 2015, "Collision model for fully-resolved simulations of flows laden with finite-size particles", *Phys Rev E*, Vol. 92, p. 053012.

[15] Metzner, A., and Reed, J., 1955, "Flow of non-newtonian fluids-correlation of the laminar, transition, and turbulent-flow regions", *AIChE Journal*, Vol. 1, pp. 434–440.

[16] El Khoury, G., Schlatter, P., Noorani, A., Fischer, P., Brethouwer, G., and Johansson, A., 2013, "Direct nulerical simulation of pipe flow at moderately high Reynolds numbers", *Flow Turbul Combust*, Vol. 91, pp. 475–495.

[17] Wilson, K., and Thomas, A., 1985, "A new analysis of the turbulent flow of non-newtonian fluids", *Canadian J of Chem Eng*, Vol. 63, pp. 539–546.

[18] Hamedi, N., and Revstedt, J., 2018, "Dynamic simulation of sedimentation of cubical particles in a power law fluid", J. Vad (ed.), *Proceedings of the 17th Conference on Fluid Flow Technologies*, paper no. CMFF18-051.